FILE

NOAA Technical Memorandum ERL PMEL-102

A CONVECTION MODEL FOR HYDROTHERMAL PLUMES IN A CROSS FLOW

J . W. Lavelle

Pacific Marine Environmental Laboratory
Seattle, Washington
July 1994

noaa NATIONAL OCEANIC AND ATMOSPHERIC ADMINISTRATION / Environmental Research Laboratories

NOAA Technical Memorandum ERL PMEL-102

A CONVECTION MODEL FOR HYDROTHERMAL PLUMES IN A CROSS FLOW

J. W. Lavelle

Pacific Marine Environmental Laboratory
Seattle, Washington
July 1994

UNITED STATES DEPARTMENT OF COMMERCE

Ronald H. Brown
Secretary

NATIONAL OCEANIC AND ATMOSPHERIC ADMINISTRATION

D. James Baker
Under Secretary for Oceans and Atmosphere/Administrator

Environmental Research Laboratories

Alan R. Thomas
Director

NOTICE

Mention of a commercial company or product does not constitute an endorsement by NOAA/ERL. Use of information from this publication concerning proprietary products or the tests of such products for publicity or advertising purposes is not authorized.

Contribution No. 1492 from NOAA/Pacific Marine Environmental Laboratory

For sale by the National Technical Information Service, 5285 Port Royal Road
Springfield, VA 22161

CONTENTS

PAGE

A Convection Model for Hydrothermal Plumes in a Cross Flow

J. W. Lavelle

ABSTRACT. A primitive equation convection model is used to describe circulatory and property fields in a region where buoyant hydrothermal fluids discharge into a rotating stratified ocean. Model results are obtained for a line source of heat and salinity which introduces buoyancy into a steady background flow. The flow bends the hydrothermal plume over and advects it downstream, but both up and downstream of the vent there is recirculation from the plume cap to the plume stem below. This circulation draws discharge-affected water downward to be reentrained into the upwardly rising water of the plume. For the given background stratification, temperature and salinity have distinctly different anomaly patterns, with that of salinity having a dipole-like distribution. Below the temperature anomaly core of the plume, a negative salinity anomaly can occur because of this downward flux. The model is used to compare plumes having differing buoyancy inputs, here specifically differences in salt content. The effects of salinity depleted discharge are to enhance the magnitude of the salinity anomaly in the lower part of the plume and to make more vigorous buoyancy-induced vertical and horizontal flows.

1. INTRODUCTION

Water column observations showing effects of hydrothermal discharge are more often than not made in the non-buoyant region of plumes (Crane *et al.*, 1985; Lupton *et al.*, 1985; Baker and Massoth, 1987; Crane *et al.*, 1988; Klinkhammer *et al.*, 1989; Rona and Speer, 1989; Coale *et al.*, 1991; Thomson *et al.*, 1992; Gendron *et al.*, 1993). The buoyant part of the plume is small compared to the much larger volume occupied by the non-buoyant mixture of hydrothermal discharge and entrained background water and it is consequently less likely to be sampled from a surface ship. Despite the preponderance of observations in the non-buoyant plume region, however, models that can properly address the distributions of properties there have, for the most part (Lavelle and Baker, 1994; Lavelle, 1994), been absent. To date most applications of theory to hydrothermal water column observations have been made using variations of the one-dimensional steady entrainment model of Morton *et al.* (1956), a model designed to address the issue of maximum rise height for given source buoyancy flux, but not the distribution of properties in the plume cap region. In this paper we present a hydrodynamical model that allows the non-buoyant plume region to be addressed. The model application here is to bent-over plumes because most field observations have been made on plumes discharging into background currents.

Several previous interpretations of hydrothermal observations have made good use of the one-dimensional theory. Converse *et al.* (1984) and Little *et al.* (1987) related observations very near the source to the buoyancy flux at the vent. The Morton *et al.* (1956) theory, which makes entrainment proportional to the vertical velocity in the plume stem, is suited to the description of the dependence of the dilution ratio on vertical distance from the vent, particularly in the lower plume stem region. Another use of the entrainment theory in a hydrothermal context has been to infer, based on the observed level of maximum rise height and background stratification, what the buoyancy flux of a megaplume source had to have been (Baker *et al.*, 1989). Despite its obvious utility in special cases, the one-dimensional steady entrainment theory provides no information on

lateral variations in a plume or on circulation in the surrounding environment. It cannot address the distribution of properties above a level where the simple entrainment theory assumption is no longer valid. This is the region of the plume cap where mixing with ambient water is no longer the result simply of horizontal entrainment.

Convective plume models of higher dimensionality can be used to overcome these limitations. In the meteorological and oceanographic literature, for example, such models are used to describe convective clouds (Kogan, 1991) and convective descent of brine at high latitude when ice leads refreeze (Smith and Morison, 1993). These models are generally time-dependent and often do not assume a hydrostatic balance of vertical forces. As in entrainment models, these models use temperature and salinity as dynamic variables and relate the plume to source conditions. Entrainment, on the other hand, is not directly parameterized; flow into the plume stem is calculated self-consistently. Assumptions about turbulent mixing replace the entrainment assumption, but an attempt is made to minimize sub grid scale effects by making that mixing as small as possible.

Here a convective plume model is used to describe a hydrothermal plume along the direction of a cross flow and with depth. The source is a line oriented normal to the flow. The description is of a starting plume having size and concentration scales similar to those observed in chronic plumes on the Juan de Fuca Ridge (Baker, 1993). The model is used to examine the combined effects of buoyancy and background flow on circulation patterns and the distributions of temperature, salinity, and tracer anomalies. Examples of the effects of varying the vent salinity are also given. Model results on the effects of the earth's rotation on circulation are similar to those reported by Speer (1989), though here a cross-flow breaks the circulation symmetry about a vertical line passing through the source point. Effects of differing rotation rates are seen by a comparison of two plumes differing only in their latitude of formation.

2. MODEL FORMULATION

Momentum and mass conservation, assuming fluid incompressibility and the validity of the Boussinesq approximation, require:

$$\frac{\partial}{\partial t}\vec{u} + \vec{u}\cdot\nabla\vec{u} = -\nabla p/\rho_0 - f\hat{k} \times \vec{u} + \nabla\cdot A\nabla\vec{u} - \hat{k}g\rho/\rho_o \tag{1}$$

$$\nabla\cdot\vec{u} = 0 \tag{2}$$

where t is the time, $\vec{u}$ consists of horizontal (u,v) and vertical velocity (w positive upward) components, p is the pressure, ρ the density, ρ_0 (1027.67 kg m^{-3}) the reference density, g (9.81 m^2 s^{-1}) the acceleration of gravity, f the Coriolis parameter, $\hat{k}$ the unit vector in the vertical direction, and A are viscosity coefficients to be described below. A hydrostatic balance is not assumed.

Conservation equations for potential temperature, θ, and salinity, S, are:

$$\frac{\partial}{\partial t}(\Theta,S) + \vec{u}\cdot\nabla(\Theta,S) = \nabla_H K_h \nabla_H(\Theta,S) + \frac{\partial}{\partial z}K_z\frac{\partial}{\partial z}(\Theta-\Theta_{BKG},S-S_{BKG}) + Q_{\Theta,S} \qquad (3)$$

Q_S represents the rate of salt discharge and Q_θ is related to the rate of heat discharge Q_H via $Q_\theta = Q_H/(\rho_o C_P)$, where C_P represents the specific heat of water (4200 J Kg^{-1} $°C^{-1}$). The variables K_h and K_z are horizontal and vertical eddy diffusivities. Note that $\Delta\theta$, ΔS rather than θ, S are diffused vertically. Otherwise vertical diffusion of θ_{BKG} and S_{BKG} profiles would occur even in a motionless system. Since the interest is the anomalies associated with hydrothermally induced motion, spurious changes in profiles must be eliminated. Alternatively this parameterization can be viewed as a method of enforcing a balance between slow vertical background advection, not part of the model, and vertical diffusion, a balance that should make θ_{BKG} and S_{BKG} profiles stationary. There are sources of heat and salt, but not mass. Upward motion is caused by buoyancy alone, i.e., there is no initial velocity at the vent and the plume is thus free rather than forced (Turner, 1979; Turner, 1986). Passive conservative tracer dispersion is governed by a like equation.

The system of equations is closed with the UNESCO equation of state (Gill, 1982). While hydrothermal fluid chemistry can be different from seawater (e.g., Butterfield *et al.*, 1990), rapid dilution after discharge lessens the importance of the differences in terms of the density approximation for the purposes of this model. The source is assumed to be linear with the consequence that model equations can be solved in two-dimensional (x-z) geometry. A background cross flow breaks the model symmetry in the x-direction. The solution is obtained numerically for a starting plume that has had time to be bent over and advected several km downstream. Middleton and Thomson (1986) also modelled bent-over hydrothermal plumes, but they used the entrainment theory approach which leaves unspecified the distributions in the non-buoyant region.

The momentum equations (Eqs. 1) are separated into three separate balances by identifying three components of pressure. The first is the hydrostatic pressure, $\tilde{P}$, arising from the weight of the stratified fluid when initially motionless. The second is a pressure, P, having constant horizontal gradients and depth dependence; this pressure forces the steady background flow that causes the hydrothermal plume to bend over. The third, a perturbation pressure p', results from the hydrothermal discharge. Variables may be separated into these mean and perturbation components:

$$\begin{aligned} p &= \tilde{P}(z) + P(x,y,z) + p'(x,z,t) \\ u &= U(z) + u'(x,z,t) \\ v &= V(z) + v'(x,z,t) \\ w &= w'(x,z,t) \\ \rho &= \rho_{BKG}(z) + \rho'(x,z,t) \end{aligned} \qquad (4)$$

Taking the source to be a line oriented along the y direction removes all y dependence from the primed variables.

The equation involving $\tilde{P}$ is a hydrostatic balance between $d\tilde{P}(z)/dz$ and $\rho_{BKG}\, g$. The second involving P defines the background flow, $\vec{U} = (U,V)$:

$$-\nabla_H P/\rho_0 - f\hat{k} \times \vec{U} + \frac{\partial}{\partial z} A_z \frac{\partial}{\partial z}(\vec{U}) = 0 \tag{5}$$

Since ∇P and A_Z have only z-dependence, Eq. 5 is analytically integrable for $\vec{U}$. If ∇P were constant in z, the solutions would be Ekman-like, with flows rotating and declining in size downward to the sea floor. In the examples to follow, however, ∇P is ramped from a constant value 100 m above to zero at the sea floor. This guarantees currents which decline from maximum values to zero over the bottom 100 m. Currents aloft are on the order of 1.5 cm s^{-1} (Cannon *et al.*, 1993) and point in a normal direction to the source; flow at the sea floor is small and aligned with the source (y-axis). Specifically, dP/dx is zero, and $(dP/dy)/(\rho_0 f)$ is 1.46×10^{-2} m s^{-1} at 100 m above the bottom. The diffusion term plays a minor role in the balance away from the sea floor given the A_z magnitude and profile described below.

The third component set of momentum equations involve perturbation velocities, pressure, and density. In flux conservative form they are:

$$\frac{\partial}{\partial t}u' + \frac{\partial}{\partial x}(u'^2) + \frac{\partial}{\partial z}(u'w') + 2\frac{\partial}{\partial x}(Uu') + \frac{\partial}{\partial z}(Uw') = -\frac{1}{\rho_o}\frac{\partial}{\partial x}p' + fv' + \frac{\partial}{\partial x}A_x\frac{\partial}{\partial x}u' + \frac{\partial}{\partial z}A_z\frac{\partial}{\partial z}u' \tag{6}$$

$$\frac{\partial}{\partial t}v' + \frac{\partial}{\partial x}(u'v') + \frac{\partial}{\partial z}(w'v') + \frac{\partial}{\partial x}(Uv' + Vu') + \frac{\partial}{\partial z}(Vw') = -fu' + \frac{\partial}{\partial x}A_x\frac{\partial}{\partial x}v' + \frac{\partial}{\partial z}A_z\frac{\partial}{\partial z}v' \tag{7}$$

$$\frac{\partial}{\partial t}w' + \frac{\partial}{\partial x}(u'w') + \frac{\partial}{\partial z}(w'^2) + \frac{\partial}{\partial x}(Uw') = -\frac{1}{\rho_o}\frac{\partial}{\partial z}p' + \rho'\frac{g}{\rho_o} + \frac{\partial}{\partial x}A_x\frac{\partial}{\partial x}w' + \frac{\partial}{\partial z}A_z\frac{\partial}{\partial z}w' \tag{8}$$

The perturbation density, ρ', is the difference of ρ and ρ_{BKG}. Mass conservation for primed variables takes the same form as Eq. 2. Acceleration terms in Eq. 8, making the description non-hydrostatic, allow for correct treatment during the plume start up. Terms involving primed and unprimed variables couple the hydrothermally forced and background flows.

Equations 3 and 6 through 8 together with the equation of state were numerically integrated over a rectangular domain with a rigid lid to determine u', v', w', p', θ and S. At the upper surface, w and the normal gradients of u, v, θ, and S were taken to be zero. Along the bottom, u, v, and w and the normal gradients of θ and S were set to zero. At each end of the region, u', v' and w' were fixed at zero; this is a statement that the plume should have no dynamical effect on flow at large distances from the vent. θ and S conditions were dependent on the sense of flow. Upstream θ and S were

assigned background values; downstream horizontal gradients of θ and S were nil. Boundary conditions for p' were determined from Eqs. 6 through 8 using the values of the other variables there (Harlow and Welch, 1965). Advection of θ and S in Eq. 3 is by the full flow, i.e., $\vec{U} + \vec{u}\,'$.

Eddy viscosity and diffusivity coefficients were taken to be temporally but not spatially invariant. Near bottom mixing coefficients were made larger than interior values as were values in sponge layers at the ends and top of the model domain (6.4 km length by 500 m depth). Sponge layers were five cells wide and there mixing coefficients, tapered to interior values, took maximum values of $1/12(dx)^2/dt$ or $1/12(dz)^2/dt$. Vertical mixing coefficients were these: A_Z was 2 $cm^2\ s^{-1}$ except in the bottom 45 m where A_Z increased from 10 to 300 $cm^2\ s^{-1}$. K_Z values were, outside of sponge layers, uniformly 2 $cm^2\ s^{-1}$. In the horizontal, A_h and K_h typically had the value 3 $m^2\ s^{-1}$. K_h at $x = 0$ and $x = L$ were set to zero to prevent diffusive flux of θ or S across the $x = 0$ and $x = L$ boundaries.

The observations of both salt enriched and low salinity discharges in hydrothermal regions (e.g., Butterfield *et al.*, 1990) motivate the initial model examination here of the corresponding plume response. This task requires that model source rates for salt, Q_S, be specified. Suppose a vent (or vent exit field) fluid has temperature θ_{VENT}, salinity S_{VENT}, and volume flux rate R. Let the discharge flow into a volume V having average temperature of approximately θ_{BKG} and salinity S_{BKG}. R is presumed to be small enough and V large enough that negligible mass and upward momentum is imported by the discharge to the fluid in volume V. Then

$$Q_H = R(\theta_{VENT} - \theta_{BKG})\,\rho_0 C_p \tag{9}$$

$$Q_S = R(S_{VENT} - S_{BKG}) \tag{10}$$

Eliminating R from equations 9 and 10 results in

$$Q_S = \frac{(S_{VENT} - S_{BKG})}{(\theta_{VENT} - \theta_{BKG})} \frac{Q_H}{(\rho_0 C_P)} \tag{11}$$

Once Q_H, θ_{VENT}, and S_{VENT} are chosen, Q_S is fixed. In examples to follow, Q_H has been assigned the value 1 MW m^{-1} so that temperature anomalies where the plume is non-buoyant would be similar to those observed on the Juan de Fuca Ridge (Baker, 1993); θ_{VENT} is assumed to be 350°C. As a consequence, when S_{VENT} = 15‰, for example, $Q_S = -1.30 \times 10^{-2}$‰ s^{-1} m^{-1}.

The equations were integrated on rectangular grid (dx = 50 m, dz = ~15 m). Background θ and S profiles, horizontally homogeneous, are based on a composite of measured profiles taken over the near-bottom depth range (1800–2300 m) in the vicinity of the Juan de Fuca ridge (Lavelle and Baker, 1994). Time stepping (dt = 10 s) was by the leap-frog method with an Asselin filter (Asselin, 1972) of coefficient 0.3 used to eliminate the second computational time mode. Equations 6 through 8 were finite differenced in the manner of Bryan (1969) so as to conserve energy. Upstream

differencing was used for θ and S (Eq. 3) and the Smolarkiewicz diffusion correction scheme (Smolarkiewicz, 1983) was employed each time step. The calculation of velocity followed the integration procedures for nonhydrostatic flow originating with Harlow and Welch (1965). Sources of heat and salt were confined to a single computational cell adjoining the bottom.

Diffusive sponge layers, as described above, were used to partially adsorb waves travelling upward and outward from the vent source to the boundaries, waves which in a perfect model would pass out of the calculational domain. End sponge layers also helped suppress instabilities at entrance and exit regions, though a slight rippling of velocities at the entrance upstream was not completely eliminated. Source rates of heat and salt were ramped from zero to maximum values over the initial 6-hour period. Abrupt start ups caused significantly more energetic waves.

3. MODEL RESULTS

3.1 Circulation

Model results are first given for the reference case: discharge occurring at 1 MW m^{-1} at 350°C with salinity that of ambient at vent depth (~34.7‰, $Q_S = 0$) and $f = 1.03 \times 10^{-4}$ s^{-1} (45°N). In Fig. 1a flow vectors ($\vec{U}+\vec{u}'$) are superimposed on a plume shadow representing the plume region in which temperature anomalies exceed 0.02°C all after 36 hours of discharge. By this time rates of change of velocity are small.

Vectors at 400 m above the bottom (Fig. 1a) represent the unperturbed background flow of 1.46 cm s^{-1}. The buoyancy-induced flow reverses the mean flow downstream of the source and cancels background flow just upstream of the source at plume cap level. Distortion of background flow occurs to a height of ~250 m under the given conditions. Upstream but near-vent-level flow is drawn downward to the base of the vent. Far upstream and downstream the plume has insignificant effects on circulation as required.

Anomalous flow, i.e., $\vec{u}'$, shows better the extent of the buoyancy-induced circulation cells (Fig. 1b). Maximum anomalous u', v', and w' velocities at this time are 4.8, 4.6 and 2.1 cm s^{-1}, respectively. Because the resolution of the source region is coarse, this vertical velocity can be compared to entrainment model values only beyond a height above the vent at which the plume has broadened to a width of 50 m (dx). Another way to view model results is to see the bottom edge of the calculational domain as beginning at a height at which a rising plume would have already broadened to a width corresponding to dx. Variable resolution gridding schemes are the road to model improvement in this regard.

Fig. 1b makes clear the recirculation of plume water from the plume cap region back into the plume stem. Entrainment models assume that only water having properties of the initial ambient profiles are entrained and these results suggest otherwise. Entraining water with only background properties may occur only near vent level (Fig. 1b). Reentrainment has consequences for the distribution of θ, S and trace metals as well as for particle and plankton transport (Mullineaux *et al.*, 1991).

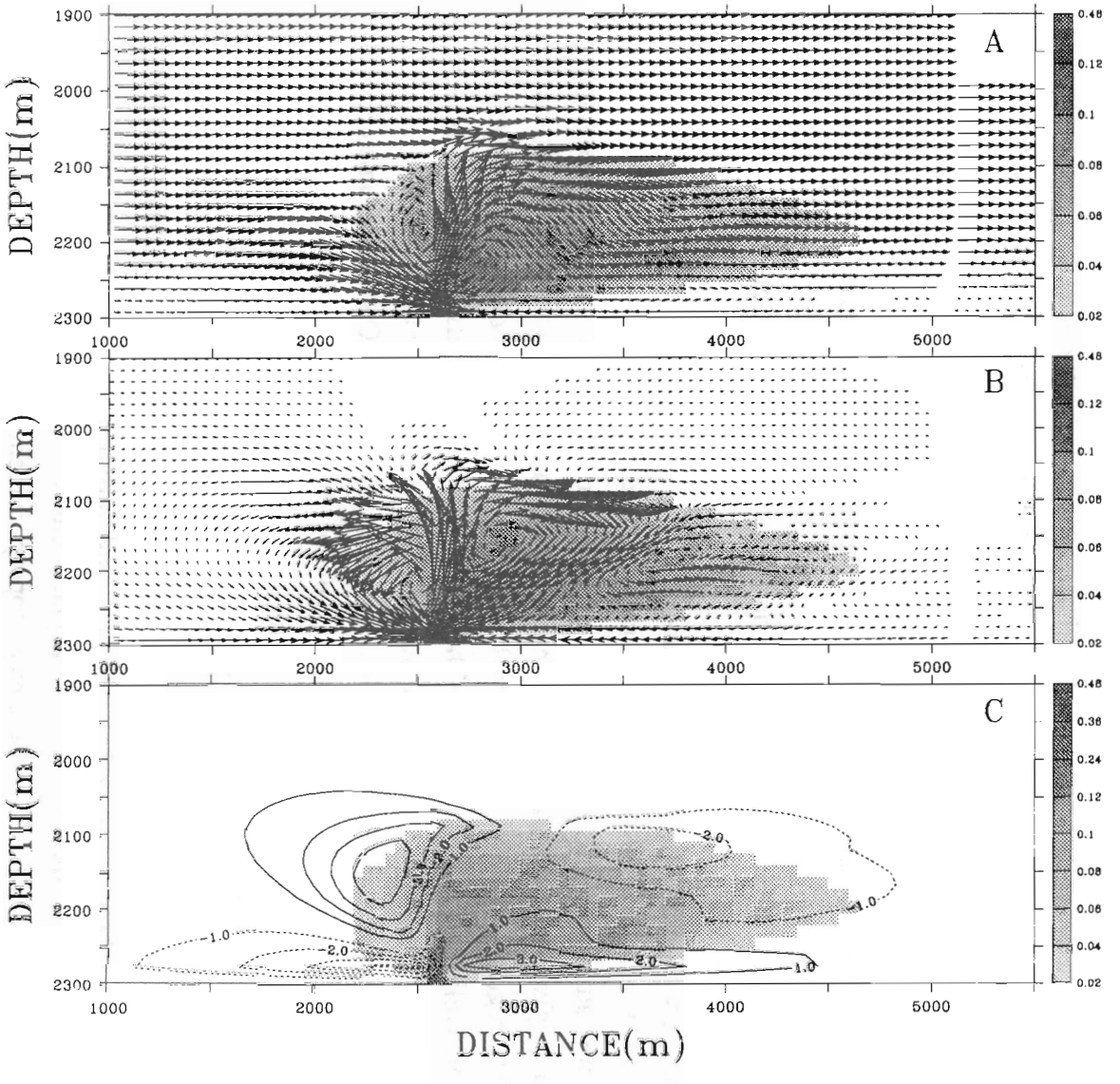

Fig. 1: Flow around a hydrothermal vent for a starting plume at age 36 hrs. Stippling represents the region where $\Delta\theta$ exceeds 0.02°C. (a) Total flow in the x-z plane in vector form; vertical flow is exaggerated by a factor of three. The background current profile has been highlighted by blanking one column of vectors; the largest vector corresponds to flow at 1.5 cm s^{-1}. Only part of the full computation domain ($0 < x < 6400$ m) is shown. (b) Flow anomaly, i.e., $\vec{u}'$, the buoyancy driven component of flow, has the same vector scale. (c) Contours of flow (cm s^{-1}) in the along-source (y) direction

Circulation effects which appear to extend to a distance of 1500 m from the source (Fig. 1b) must be viewed with caution. The geometry of the source is likely to be a significant factor. A line source should cause apparent flow effects to extend greater distances than is likely for a point source, given the same buoyancy flux. For a point source, the return flow is omnidirectional and the magnitude of the inward flow near the bottom should diminish more rapidly with distance from the vent.

The effects of rotation are evident in induced flow in the along-source direction (Fig. 1c). Flow in the positive y-direction is paired both laterally and vertically with flow in the opposite direction. Flow magnitudes as large as 4.6 cm s^{-1} are predicted for this line source. Cross-flow in the x-direction breaks the symmetry of these patterns about a vertical line through the source. Effects of rotation on hydrothermal plumes were first examined by Speer (1989).

Anomalous pressure p' distribution for the same examples (Fig. 2a) shows a low pressure anomaly around the plume base and high pressure anomaly in the plume cap region. The horizontal pressure gradient dp/dx (Fig. 2a, stippled) are high were u' velocities are high (Fig. 1b and Eq. 5a). High pressure drives flow outward in the x-direction in the plume cap and Coriolis forces bend that flow to the right ($f = 1.03 \times 10^{-4}$ s^{-1}, 45°N).

The density anomaly (Fig. 2b, stippled) shows a small region of elevated density more than 200 m above the seafloor and a much larger region of reduced density. The reduction is caused by elevated temperature and reduced salinity which results from the downward recirculation into the plume stem. Isopycnals are drawn downward into the stem and bowed upward well above the source (Fig. 2b). The region (not shown) of positive buoyancy, that is negative $d\rho/dz$, extends vertically and in a relatively narrow column above the source and then spreads slightly and primarily downstream just below the positive density anomaly, i.e., to ~2100 m in this example.

The effects on circulation and temperature anomaly for a variable Coriolis parameter, f, may be inferred from Fig. 3. The comparison is between plumes formed at 45°N ($f = 1.03 \times 10^{-4}$ s^{-1}) and ~4°N ($f = 1.03 \times 10^{-5}$ s^{-1}). Fig. 3a shows the plume of Fig. 1, but at 16 hours; time was chosen with regard to the size of the second plume. The plume in Fig. 3b, formed where the rotation rate is smaller, extends farther outward from the source. The streamfunctions associated with the velocity anomalies, u' and w', indicate the reason (Fig. 3). With diminished rotation, the circulation reaches a greater distance in the x-direction. Flow which would have been directed by a stronger Coriolis force into the along source direction pushes the plume outward. Even near the sea floor where the width of the plume stem might be considered an appropriate length scale, rotational effects are felt (e.g., Fig. 1c) because that circulation is coupled to the flow aloft by continuity and angular momentum conservation. Rotational effects are not included in typical entrainment models because that model focuses on the plume stem region.

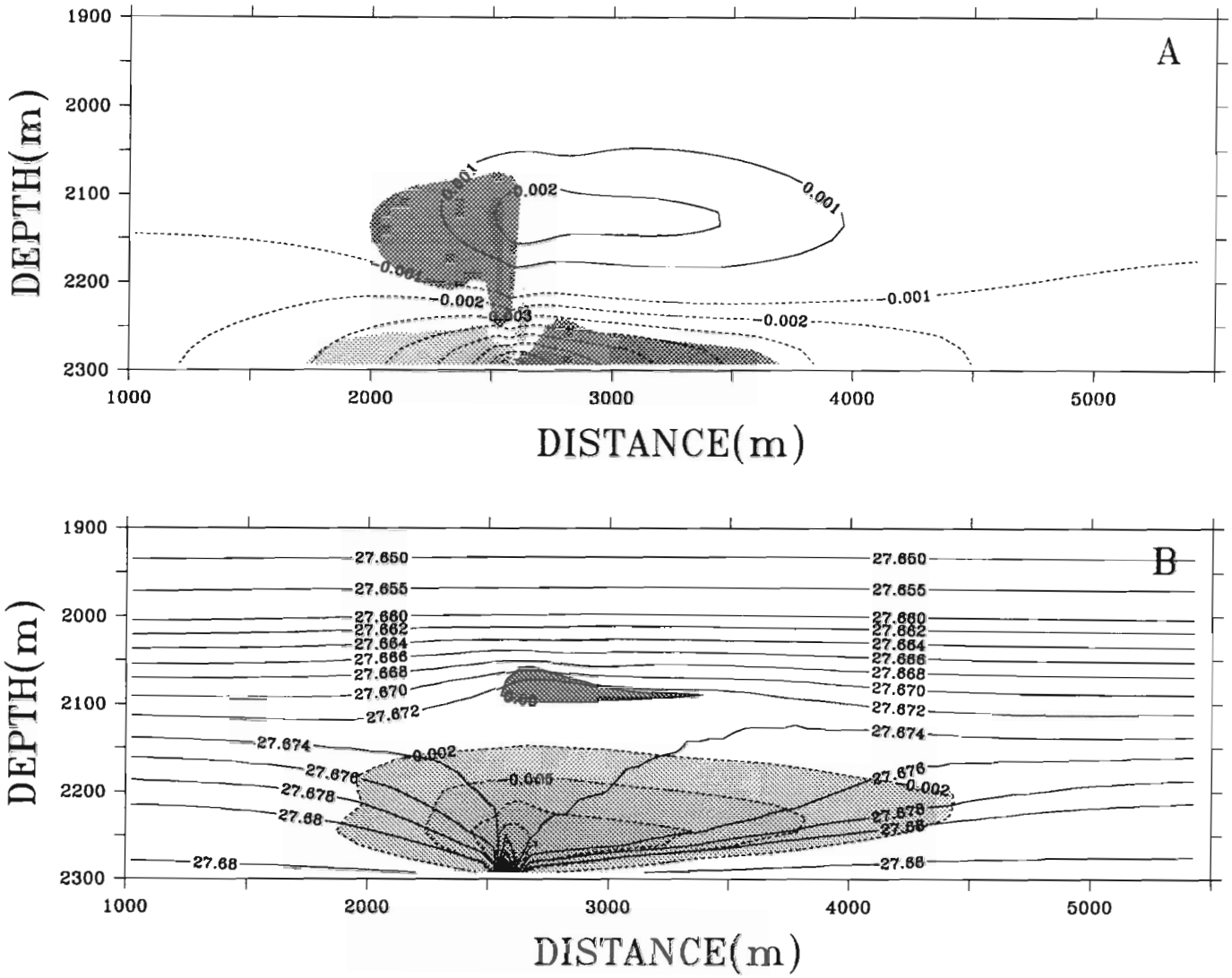

Fig. 2: (a) Contours of anomalous pressure p' driving the buoyancy flow (Fig. 1b). Dark stippling show regions of positive dp'/dx and light stippling those of negative dp'/dx (Eq. 8). (b) The density anomaly associated with the ϑ and S distributions (Fig. 4). Dark stippling is a region of positive and lighter stippling a region of negative density anomaly. Contours of σ_0 are overlain.

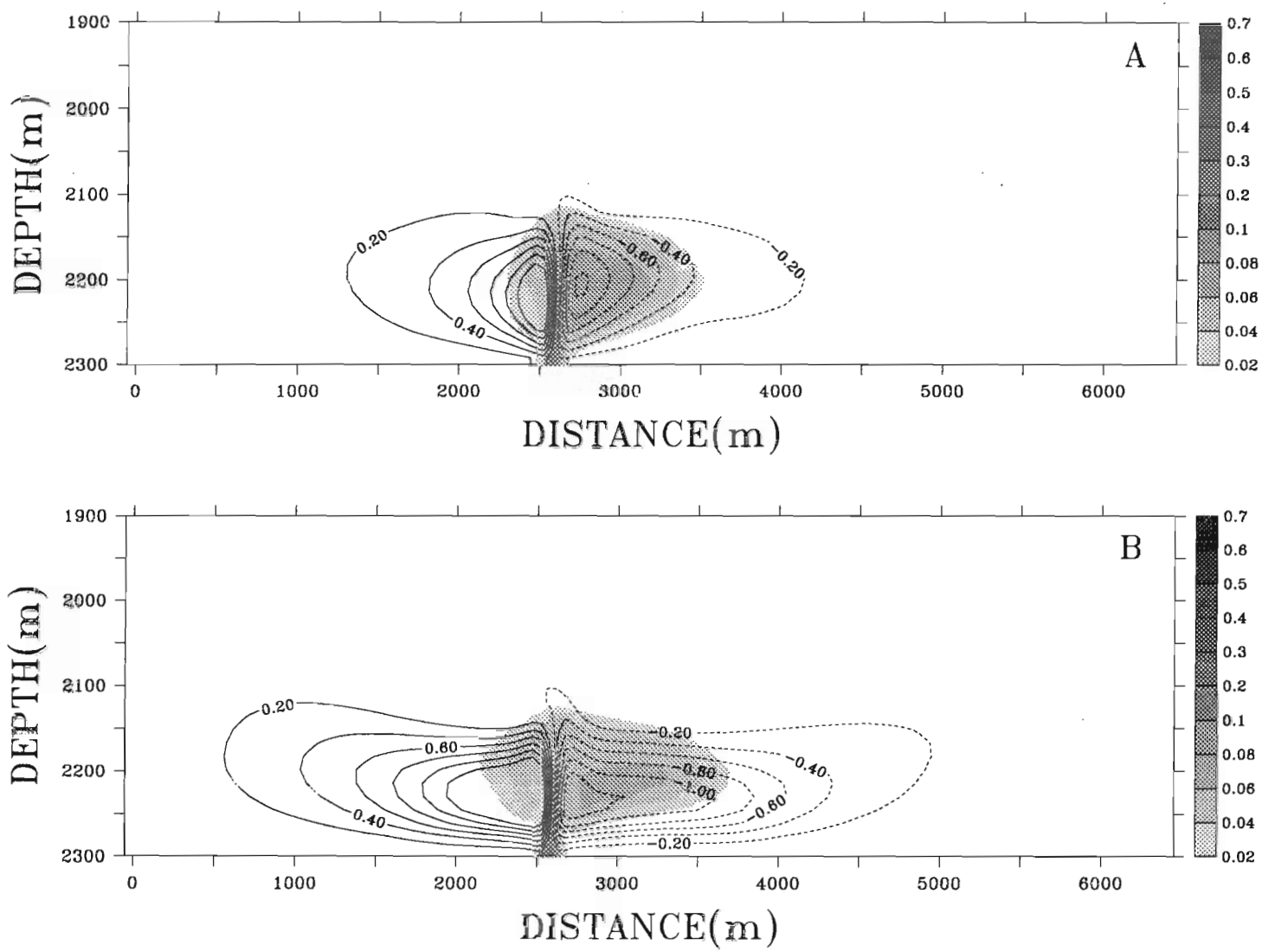

Fig. 3: A comparison of starting plumes at 16 hrs for different rates of rotation: (a) $f = 1.03 \times 10^{-4}$ s^{-1} (45°N) and (b) $f = 1.03 \times 10^{-5}$ s^{-1} (~4°N). Contours are streamlines of buoyancy-driven flow components.

3.2 Property fields

Advection by the flow field of Fig. 1 rearranges local ambient heat and salt fields. Figure 4 shows θ, S, and tracer concentration anomalies (e.g., $\Delta\theta = \theta - \theta_{BKG}$) after 36 hours of discharge under reference case conditions. For a free stream advection speed of 1.46 cm s^{-1}, the downstream extent of the thermal plume (0.02°C $\Delta\theta$ boundary) is nearly 2 km. The plume also extends upstream of the vent, a consequence of buoyancy-induced circulation as well as diffusion. Plume thickness near the source is about 200 m. The plume stem is short and thick after 36 hours for these reasons: 1) the spatial resolution of the model is currently uniform horizontally and vertically and is coarse with regard to the size of the actual plume stem. 2) Downward recirculation in a line-source model slowly fills the downstream underside of the plume with discharge-affected water. If the source were a point and the calculation 3-dimensional, this would be unlikely. 3) Numerical calculations in regions of high property gradients have difficulty preventing unwanted numerical diffusion (Smolarkiewicz and Grabowski, 1990).

The ΔS pattern (Fig. 4b) shows a region of positive salt anomaly high in the water column which results from the upward advection of relatively salt enriched water from depth (see Fig. 6 for background profiles). The recirculating flow has done the inverse: water of lower salinity is brought downward from above to create a negative salt anomaly below. The symmetry-breaking cross flow causes that negative salt anomaly to be much larger upstream of the source than downstream where less background-like water is recirculated downward. Because there is no discharge in the reference case ($Q_S = 0$), the salt anomaly pattern represents the redistribution of ambient water. Profiles taken within Megaplume I (Lavelle and Baker, 1994) show negative salinity anomalies in their lower part.

Does the positive salt anomaly above the region of positive buoyancy persist past the early formation stages? It does. The rate of change of salinity near the anomaly maximum at ~2100 m is negligible after ~16 hours. The gradient of vertical flux, the indicator of how the anomaly is being supplied, shows a narrow stream of positive salt flux that reaches from ~60 m above the vent directly into the positive anomaly region. Entrainment and buoyant convection together sustain a positive salinity anomaly, as noted by Lupton *et al.* (1985).

A tracer having no role in the dynamics and one for which the background is unstratified is found to have a plume (Fig. 4c) unlike that of either heat or salt. Neither tracer-temperature or tracer-salt plumes are congruent. Congruency would occur if θ and S had no background gradients, in which case no level of non-buoyancy could be achieved, or if the tracer background were stratified like either θ or S.

Results for discharge at a salinity of 15‰ were obtained under conditions identical to those of the reference case save that Q_S was given a value -1.30×10^{-2}‰ s^{-1} m^{-1}. Results on flow (not shown) confirm a more vigorous buoyancy flow and stronger along-source Coriolis-induced currents (max of 6 cm s^{-1} versus 4.6 cm s^{-1} for the reference case) as were to be expected. Temperature, salinity and density anomalies (Fig. 5) confirm a higher rise height. In comparison to the reference case (Fig. 5, stippled), the positive salt anomaly is shifted upward about 50 m and has a maximum

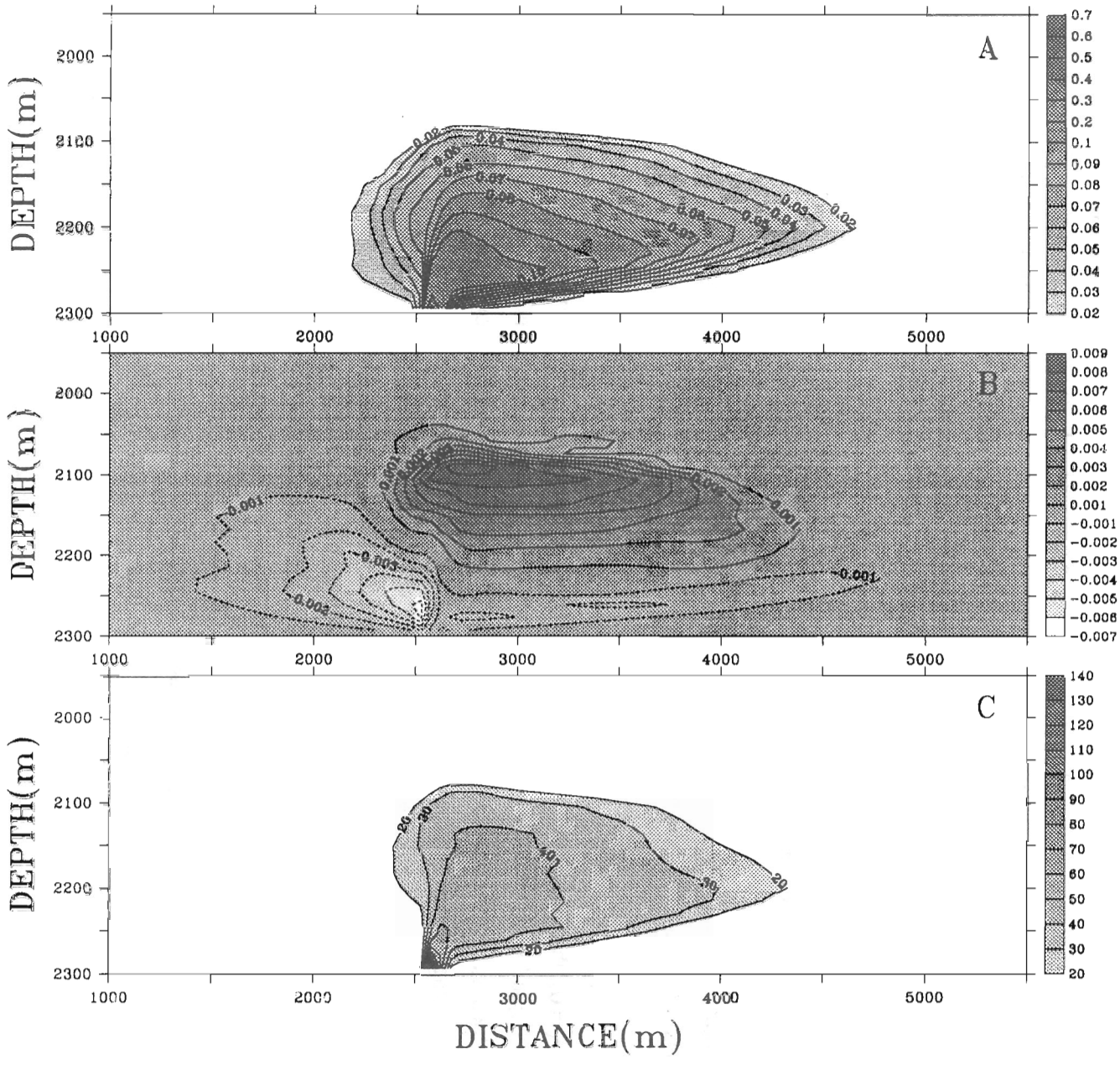

Fig. 4: For the reference plume at 36 hrs, (a) $\Delta\vartheta$ at intervals of .01°C; (b) ΔS at intervals of .001‰, and (c) conservative tracer concentrations in arbitrary units.

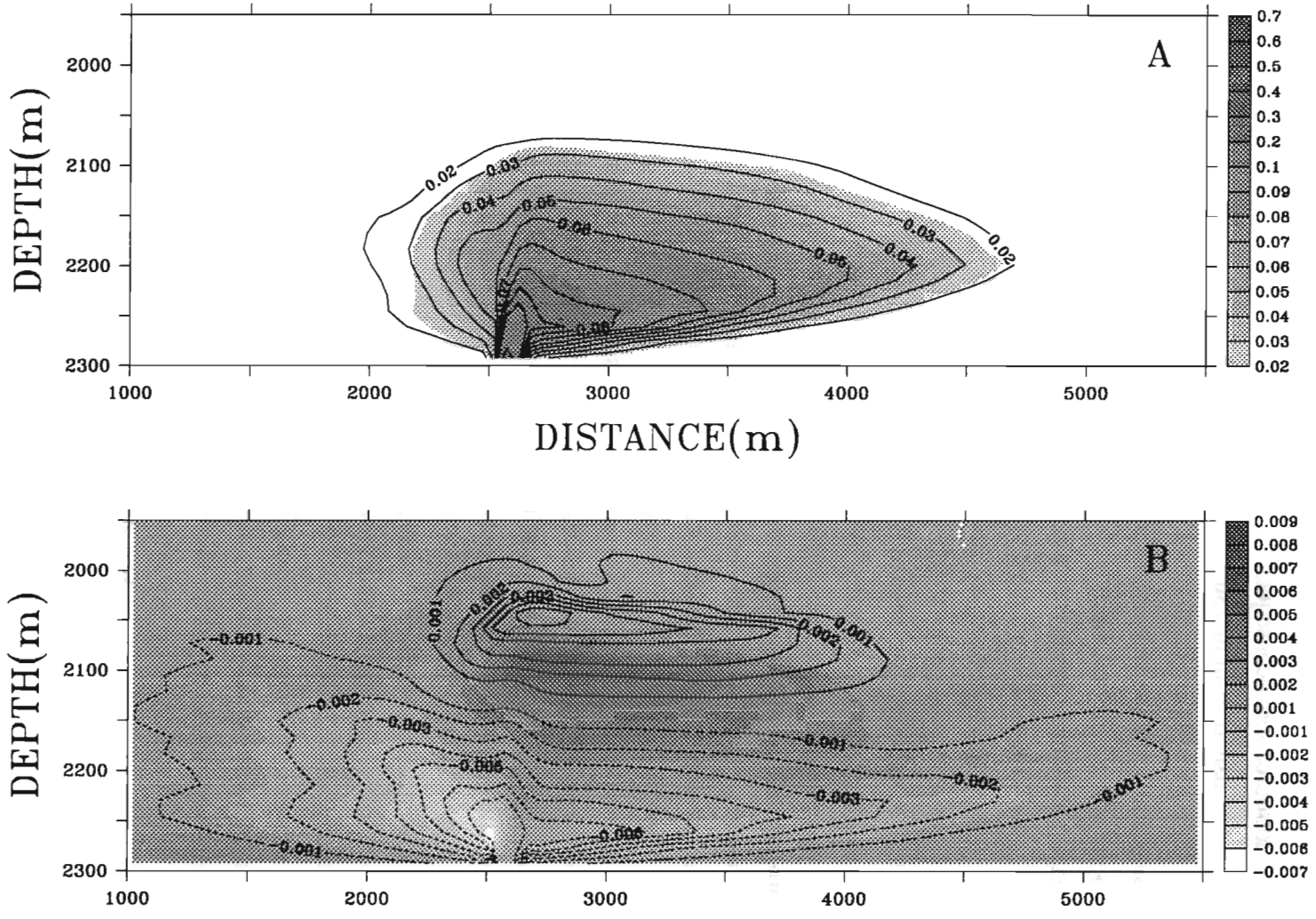

Fig. 5: Comparison of temperature and salinity anomalies for vent effluent having (a) ambient salinity (stippled) (b) a salinity of 15‰ (contoured).

value slightly higher than the reference case (.0077 vs .0068‰). The negative anomaly maximum is more than twice the reference level (.0163 vs. .0063‰). In contrast the differences in the distributions of temperature are not appreciably different.

Profiles through both plumes at 300 m downstream (Figs. 6a and 6b) and 200 m (Figs. 6c and 6d) upstream of the source show consequences of varying source salinity. Background profiles (solid lines, Fig. 6) are composited from measured profiles from the Juan de Fuca Ridge which had been judged to show little hydrothermal influence. Profiles for the reference discharge are represented by dotted line and profiles in the case of discharge with 15‰ salinity are given by dashed lines. For the given background conditions, salinity profiles (Figs. 6a and 6c) all show intervals of both positive and negative anomaly while θ profiles (Figs. 6b and 6d) have barely perceptible negative anomalies only above 2100 m. Downstream of the source (Figs. 6a and 6b) profiles have only slight gradients between 40 m above bottom and 2100 m while upstream (Figs. 6c and 6d) the same does not hold. The two-dimensional geometry chosen for source and model and the consequent nature of downward reentrainment shapes these profiles.

Based on profiles in Fig. 6, it would appear that differences in salinity content of discharge along the Juan de Fuca Ridge are much more likely to be detectible in salinity profiles than in temperature profiles, even though temperature too is subject to more vigorous circulation caused by the increased buoyancy. In the model, low salinity discharge causes larger negative anomalies in the lower part of the water column, but it does not change the occurrence of a positive salinity anomaly higher up. Consequently, looking for differences in source salinity in water column signals should begin with salt anomalies near bottom. The anomalies are small and the difficulty of identifying background profiles may make the task difficult, however, in the case of field data.

At several points in this work features in the results that are likely the consequence of the dimensionality of the source and model have been acknowledged. One circumstance that has been unavoidable is that after sufficiently long simulation times the entire region between the non-buoyant plume and the bottom fill with discharged-influence water. Somewhat before this, the plume stem unrealistically broadens in the downstream direction. Results presented have been for a starting plume of at most 36 hours duration for this reason, though the simulation has been run well beyond this time. The source of these difficulties lies in the fact that return flow to the plume stem, in two dimensions, can only come from the upstream and downstream directions. Once the plume advecting downstream crosses the downstream boundary, all downstream downward flow, which is needed for continuity, must transport plume-influence water. In three dimensions, return flow to the stem is omnidirectional and this effect does not occur. By limiting results to times that are short compared to the time to advect to the downstream boundary, these effects are mitigated but a realistic steady state cannot be obtained in two-dimensions.

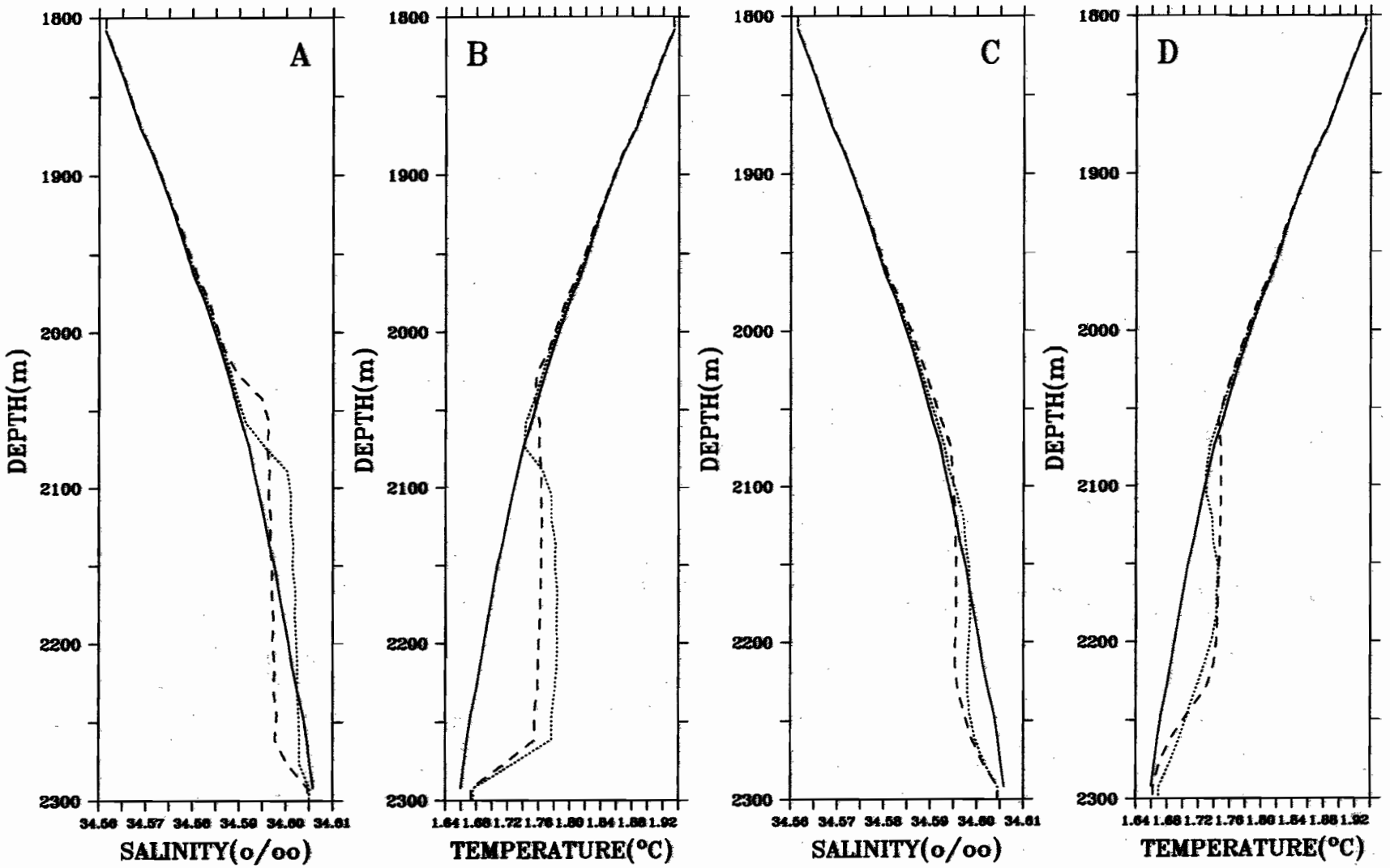

Fig. 6: Profiles of salinity and temperature 300 m downstream (A and B) and 200 m upstream (C and D) of vents discharging at two different salinities. Solid lines represent ambient conditions on the Juan de Fuca Ridge (in 1986). The dotted line is the case of reference discharge (S = 34.7‰, the ambient salinity) and the dashed line the case of discharge at reduced (15‰) salinity.

4. CONCLUSIONS

While individual results are specific to the source and model geometry and background environment, certain general conclusions can be drawn. First, temperature and salinity, both quantities that affect the plume dynamics, have different anomaly patterns. The model shows a salinity anomaly dipole. For Juan de Fuca Ridge background profiles, a positive salinity anomaly occurs above and a negative anomaly below the core of the temperature anomaly. Downward advection of less saline water in the periphery of the plume and the transport of more saline water upward in the rising plume is the cause. The resulting non-congruency of temperature and salinity anomalies is almost certain to hold true in other stratification conditions.

Reentrainment of discharge-affected water into the upward rising plume must be expected. Reentrainment has consequences for the distribution not only of heat, salt, and chemical species emanating from a vent (vent field) but it has consequences for slowly settling particles and biota that are slowly swept into the upwardly rising flow above the vent.

The earth's rotation can be factor in circulation and plume configuration even for plumes which rise only a few hundred meters into the water column. Horizontal length scales in the plume cap for chronically discharging plumes become large enough that Coriolis force becomes significant in the overall force balance. Flow transverse to the anomalous pressure gradients then develops. Because flow in the plume cap region is connected by continuity and angular momentum conservation with flow near bottom, deep flow around the vent will respond as well. The intensity of discharge, among other factors, will determine the corresponding rotational flow intensity and hence whether it is measurable.

A convection model for hydrothermal plumes unites information about source rates, plume distributions and the buoyancy forced circulation in a natural way. Having a model which addresses distributions in the plume cap region is particularly important because most of the field measurements are taken there. The work here shows the feasibility of the approach and the potential use of a convection model as an interpretative tool. Needless to say, the model does not replace the entrainment theory, which has been extraordinarily successful in a plethora of physical settings. The Morton *et al.* (1956) theory and its variants will continue to be used in hydrothermal work with regard to estimates of maximum rise height and entrainment and dilution within the plume stem for points below which the entrainment assumption is still reasonable. When the interest moves beyond the buoyant plume region to the distribution of properties in the plume cap or to the circulation in the surrounding environment and their relationship to source conditions, a convection model like the one described here will serve the purpose.

5. ACKNOWLEDGMENTS

The research is supported by the NOAA VENTS program. I thank Ed Baker and Gary Massoth for many helpful discussions about hydrothermal plumes, Michael Spillane for his comments on the work, and Steve Hankin for his data analysis package FERRET. Contribution 1492 from NOAA/Pacific Marine Environmental Laboratory.

6. REFERENCES

Asselin, R.A. (1972): Frequency filters of time integrations. *Mon. Wea. Rev., 100*(6), 487–490.

Baker, E.T. (1993): A 6-year time series of hydrothermal plumes over the Cleft segment of the Juan de Fuca Ridge. *J. Geophys. Res., 99*(B3), 4889–4904.

Baker, E.T., J.W. Lavelle, R.A. Feely, G.J. Massoth, S.L. Walker, and J.E. Lupton (1989): Episodic venting of hydrothermal fluids from the Juan de Fuca Ridge. *J. Geophys. Res., 94*, 9237–9250.

Baker, E.T., and G.J. Massoth (1987): Characteristics of hydrothermal plumes from two vent fields on the Juan de Fuca Ridge, northeast Pacific Ocean. *Earth. Planet. Sci. Lett., 85*, 59–73.

Bryan, K. (1969): A numerical method for the study of the circulation of the world ocean. *J. Comp. Phys., 4*, 347–376.

Butterfield, D.A., G.J. Massoth, R.E. McDuff, J.E. Lupton, and M.D. Lilley (1990): Geochemistry of hydrothermal fluids from Axial Seamount Hydrothermal Emissions Study vent field, Juan de Fuca Ridge: Subseafloor bioling and subsequent fluid-rock interaction. *J. Geophys. Res., 95*(B8), 12,895–12,921.

Cannon, G.A., D.J. Pashinski, and M. Lemon (1993): Hydrothermal effects west of the Juan de Fuca Ridge. *Deep Sea Res., 40*(7), 1447–1457.

Coale, K.H., C.S. Chin, G.J. Massoth, K.S. Johnson, and E.T. Baker (1991): In-situ chemical mapping of dissolved iron and manganese in hydrothermal plumes. *Nature, 352*, 325–328.

Converse, D.R., H.D. Holland and J.M. Edmond (1984): Flow rates in the axial hot springs of the East Pacific Rise (21°N): Implications for the heat budget and the formation of massive sulfide deposits. *Earth Planet. Sci. Lett., 69*, 159–175.

Crane, K., F. Aikman III, R. Embley, S. Hammond, A. Malahoff, and J. Lupton (1985): The distribution of geothermal fields on the Juan de Fuca Ridge. *J. Geophys. Res., 90*, 727–744.

Crane, K., F. Aikman III, and J.-P. Foucher (1988): The distribution of geothermal fields along the East Pacific Rise from 13°10′N to 8°20′N: Implications for deep-seated origins. *Mar. Geophys. Res., 9*, 211–236.

Gendron, J. F., J.F. Todd, R.A. Feely, E.T. Baker, and D. Kadko (1993): Excess Rn^{222} over the Cleft segment, Juan de Fuca Ridge. *J. Geophys. Res., 99*(B3), 5007–5015.

Gill, A.E. (1982): *Atmospheric-oceans dynamics*. Academic Press, New York.

Harlow, F.H., and J.E. Welch (1965): Numerical calculation of time-dependent viscous incompressible flow of fluid with a free surface. *Phys. Fluids, 8*(12), 2182–2189.

Klinkhammer, G., H. Elderfield, M. Greaves, P. Rona, and T. Nelsen (1989): Manganese geochemistry near high-temperature vents in the Mid-Atlantic Ridge rift valley. *Earth Planet. Sci. Lett., 80*, 230–240.

Kogan, Y.L. (1991): The simulation of a convective cloud in a 3-D model with explicit microphysics. Part I: model description and sensitivity experiments. *J. Atmos. Sci., 48*(9), 1160–1189.

Lavelle, J.W. (1994): The initial rise of a hydrothermal plume from a line segment source—results from a three-dimensional model. *Geophys. Res. Lett.*, in press, 1994.

Lavelle, J.W., and E. Baker (1994): A numerical study of local convection in the benthic ocean induced by episodic hydrothermal discharges. *J. Geophys. Res.*, in press, 1994.

Little, S.A., Stolzenbach, K.S. and R.P. von Herzen (1987): Measurements of plume flows from a hydrothermal vent field. *J. Geophys. Res., 92*, 2587–2596.

Lupton, J.E, J.R. Delaney, H.P. Johnson, and M.K. Tivey (1985): Entrainment and vertical transport of deep-ocean water of buoyant hydrothermal plumes. *Nature, 316*, 621–623.

Middleton, J.M. and R.E. Thomson (1986): Modelling the rise of hydrothermal plumes. Canadian Technical Report of Hydrography and Ocean Science, No. 69, Inst. of Ocean Sciences, Sidney, B.C., 18 pp.

Morton, J.L., G. Taylor, and J.S. Turner (1956): Turbulent gravitational convection from maintained and instantaneous sources. *Proc. Royal. Soc., Ser. A., 234*, 1–23.

Mullineaux, L.S., P.H. Wiebe, and E.T. Baker (1991): Hydrothermal vent plumes: larval highways in the deep sea? *Oceanus, 34*(3), 64–68.

Rona, P.A., and K.G. Speer (1989): An Atlantic hydrothermal plume: Trans-Atlantic Geotraverse (TAG) area, Mid-Atlantic Ridge crest near 26°0′N. *J. Geophys. Res., 94*, 13,879–13,893.

Smith IV, D.C., and J. Morison (1993): A numerical study of halocline convection beneath leads in sea ice. *J. Geophys. Res., 98*(C6), 10,069–10,084.

Smolarkiewicz, P. (1983): A fully multidimensional positive definite advection transport algorithm with small implicit diffusion. *J. Comp. Phys., 54*, 325–362.

Smolarkiewicz, P.K., and W.W. Grabowski (1990): The multidimensional positive definite advection transport algorithm: non-oscillatory option. *J. Comp. Physics., 86*(2), 355–375.

Speer, K.G. (1989): A forced baroclinic vortex around a hydrothermal plume. *Geophys. Res. Lett, 16*(5), 461–464.

Thomson, R.E., J.R. Delaney, R.E. McDuff, D.R. Janecky, and J.S. McClain (1992): Physical characteristics of the Endeavor Ridge hydrothermal plume during July 1988. *Earth Planet. Sci. Lett., 111*, 141–154.

Turner, J. (1979): *Buoyancy in Fluids*. Cambridge Univ. Press, Cambridge, 369 pp.

Turner, J.S. (1986): Turbulent entrainment: the development of the entrainment assumption and its application to geophysical flows. *J. Fluid Mech., 173*, 431–471.

*U.S. GOVERNMENT PRINTING OFFICE:1994-573-013/00031